Applied Thermal Engineering 50 (2013) 816–825

Contents lists available at SciVerse ScienceDirect

Applied Thermal Engineering

journal homepage: www.elsevier.com/locate/apthermeng

Thermodynamic analysis and optimization of a solar-driven regenerative organic Rankine cycle (ORC) based on flat-plate solar collectors

Man Wang [a], Jiangfeng Wang [a,*], Yuzhu Zhao [b], Pan Zhao [a], Yiping Dai [a]

[a] Institute of Turbomachinery, School of Energy and Power Engineering, No.28 Xianning West Road, Xi'an Jiaotong University, Xi'an 710049, China
[b] China HuaDian Electric Research Institute, Hangzhou 310030, China

HIGHLIGHTS

- A solar-driven regenerative ORC using flat-plate solar collectors is simulated.
- Sensitivity analysis of parameters and parameter optimization are conducted.
- The daily average efficiency is defined to evaluate the system performance.

ARTICLE INFO

Article history:
Received 2 February 2012
Accepted 10 August 2012
Available online 23 August 2012

Keywords:
Flat-plate collector
Optimization
ORC
Parametric analysis
Solar energy

ABSTRACT

This paper presents a regenerative organic Rankine cycle (ORC) to utilize the solar energy over a low temperature range. Flat-plate solar collectors are used to collect the solar radiation for their low costs. A thermal storage system is employed to store the collected solar energy and provide continuous power output when solar radiation is insufficient. A daily average efficiency is defined to evaluate the system performance exactly instead of instantaneous efficiency. By establishing mathematical models to simulate the system under steady-state conditions, parametric analysis is conducted to examine the effects of some thermodynamic parameters on the system performance using different working fluids. The system is also optimized with the daily average efficiency as its objective function by means of genetic algorithm under the given conditions. The results indicate that under the actual constraints, increasing turbine inlet pressure and temperature or lowering the turbine back pressure could improve the system performance. The parametric optimization also implies that a higher turbine inlet temperature with saturated vapor state could obtain the better system performance. Compared with other working fluids, R245fa and R123 are the most suitable working fluids for the system due to their high system performance and low operation pressure.

1. Introduction

With the increasing development of science and technology, demand for energy is surging at an unprecedented pace. Considering the growing consumption of conventional primary energy (coal, petroleum, natural gas) and environment-related concerns, recovering low temperature heat sources has become an inevitable option to solve the energy and environment problem.

ORC as a promising energy conversion technology in the field of low grade heat utilization has been studied by many researchers for decades [1,2]. In recent years, some researchers have paid more attention to employing organic Rankine cycle to utilize solar energy for its abundant and sustainable resource. Li and Pei et al. [3] proposed a low temperature solar thermal electric system which consisted of compound parabolic concentrator (CPC) with a small concentration ratio and organic Rankine cycle with R123. Phase change materials (PCMs) were added to the system to store collected energy maintaining the stability of power output. They [4] also employed regenerative organic Rankine cycle instead of basic ORC to improve the system efficiency. Quoilin et al. [5] presented the design of a solar organic Rankine cycle installed in Lesotho. The system consisted of parabolic trough collectors, a thermal storage tank, and a small-scale ORC system using scroll expanders. With conservative hypotheses and real expander efficiency curve, the overall electrical efficiency of the system could reach 7% and 8%. From the above mentioned investigations, the concentrating collectors were usually used to collect solar radiation and they were more expensive than the flat plate collector.

* Corresponding author. Tel./fax: +86 029 82668704.
E-mail address: jfwang@mail.xjtu.edu.cn (J. Wang).

1359-4311/$ – see front matter © 2012 Elsevier Ltd. All rights reserved.
http://dx.doi.org/10.1016/j.applthermaleng.2012.08.013

Nomenclature

A	area, m^2
C	specific heat capacity, kJ kg^{-1} K^{-1}
D	diameter, m
F'	collector efficiency factor
F_R	heat removal factor
h	enthalpy, kJ kg^{-1}; convective heat transfer coefficient, W m^{-2} K
I	hourly radiation, W m^{-2}
k	thermal conductivity of the insulation
L	length, m
m	mass flow rate, kg s^{-1}
M	number of glass covers
n	the day of the year
p	pressure, MPa
Q	heat rate, kW
R	tilt factor for radiation
s	entropy, kJ kg^{-1} K^{-1}
S	incident solar flux, W m^{-2}
T	temperature, °C
U	loss coefficient, W m^{-2} K^{-1}
W	power, kW; pitch of tube, m

Greek letters

α	absorptivity
β	collector tilt angle, °
δ	declination, °; thickness, m
ε	emissivity for long wave length radiation
η	efficiency
θ	angle of incidence, °
ρ	destiny, kg m^3; reflectivity
τ	transmissivity; time, s
ϕ	latitude, °
ω	hour angle, °

Subscripts

a	ambient
b	beam radiation; bottom
c	covers
cond	condenser
d	diffuse radiation; daily
i	inside
in	input
instant	instant
fi	inlet of solar collector
fo	outlet of solar collector
load	load
loss	loss;
L	heat storage tank
net	net
o	outside
out	output
p	absorber plate
pm	average value
pw	water
P	pump
R	Rankine cycle
s	side; isentropic
t	top; tank
T	turbine
u	useful
w	water
w1	water

Wang et al. [6] conducted an experimental study to investigate the performance of a low-temperature solar Rankine cycle using R245fa as working fluid. A flat plate solar collector and an evacuated solar collector were used to collect solar radiation together, and a rolling-piston expander was mounted in the system. They [7] also built another experimental system consisting of a flat plate collector, a throttling valve, a pump and an air cooled condenser, to investigate the performance of solar Rankine cycle. Some researchers [8–18] coupled a solar-driven ORC with a reverse osmosis (RO) desalination sub-system to achieve the water purification from seawater or to remove the salt and other substances from the water. The solar-powered ORC transformed the solar radiation into mechanical power and the useful shaft power was used to drive the high pump of the RO unit. The existing installed solar ORC system usually didn't contain a thermal storage system. If the solar-ORC-RO systems used the thermal storage system to store the solar energy, they could operate continuously day and night, avoiding startup and shutdown of ORC system frequently.

In a solar-powered ORC system, choosing suitable working fluids is also a critical factor for achieving an efficient and safe operation. Not only thermophysical properties, but also chemical stability, environment impact and cost need to be considered to match the application. Therefore, much attention has been focused on the working fluid selection for solar-powered ORC system. Tchanche et al. [19] conducted the selection of most suitable fluids for a low-temperature solar ORC. By evaluating and comparing 20 potential working fluids, they pointed out that R134a appeared as the most suitable for small solar application. Rayegan et al. [20] developed a procedure to compare capabilities of working fluids employed in solar Rankine cycles with similar operation conditions. Results showed that 11 fluids were suggested to be used in solar ORCs that used low or medium temperature solar collectors.

Since the pure fluids were vaporized at a constant temperature, resulting in a thermal mismatch between working fluid and sensible heat source, mixture fluids were recommended to be used in ORC for its varied temperature evaporation behavior. Wang et al. [21] analyzed some zeotropic mixtures theoretically in low temperature solar Rankine cycles for power generation, and pointed out that using zeotropic mixture could obtain a significant increase of thermal efficiency and extend the range of choosing working fluids. They [22] also conducted a comparative study of pure fluids and zeotropic mixtures in the experimental condition. The results showed that the collector efficiency and thermal efficiency of zeotropic mixtures (R245fa/R152a) were higher than that of R245fa and indicated that zeotropic mixtures had the potential for overall efficiency improvement. Bao et al. [23] proposed a novel auto-cascade low-temperature solar Rankine cycle using zeotropic mixture (isopentane/R245fa) as working fluid. Results showed that the thermal efficiency of the proposed cycle using a mixture of 32% R245fa was significantly higher than that of the single stage low temperature solar Rankine cycle.

In this study, we have developed a solar low-temperature regenerative ORC power generation system based on flat plate collector using selected organic working fluids, namely, R245fa, R123, isobutane, R134a. In order to obtain a steady power output when the solar energy is insufficient in cloudy days or at nights, a thermal storage tank has been integrated into the system. A daily average efficiency as a modified system efficiency is defined to evaluate the system performance exactly instead of the instantaneous efficiency. A parametric analysis is conducted to examine the

effects of some thermodynamic parameters on the system performance. The solar-driven power generation system is also optimized with the daily average efficiency as its objective function by means of genetic algorithm to achieve the optimum performance under the given conditions.

2. System description and selection of working fluids

The solar-driven regenerative ORC system consists of a solar energy collecting subsystem, a thermal storage subsystem and an organic Rankin cycle subsystem. Fig. 1 illustrates the schematic diagram of the entire system. The major part of the solar energy collecting system is the array of flat-plate solar collectors for its low cost and wide application. The thermal storage tank is employed to store the collected solar energy and to provide stable power output when solar radiation is insufficient. The booster heater is installed as the backup energy source to boost the temperature of thermal storage tank to the allowable temperature when the temperature of thermal storage tank drops below the reference temperature. Water is used in both the solar energy collector system and the thermal storage system.

The organic Rankine cycle subsystem mainly consists of five components, namely, a vapor evaporator, a turbine, a condenser, a pump and a regenerator. Fig. 2 illustrates *T*–*s* diagram of the solar-driven regenerative ORC system, which is composed of the following processes:

3–4: an isobaric heat absorption process in the vapor evaporator;
4–5s: an isentropic expansion process through the turbine;
4–5: an actual expansion process through the turbine;
5–6: an isobaric heat rejection process in the regenerator;
6–1: an isobaric heat rejection process in the condenser;
1–2s: an isentropic compression process in the pump;
1–2: an actual compression process in the pump;
2–3: an isobaric heat absorption process in the regenerator.

Liquid organic working fluid from condenser is compressed by the pump and fed to the vapor evaporator after preheated in regenerator. It is then evaporated in the vapor evaporator and

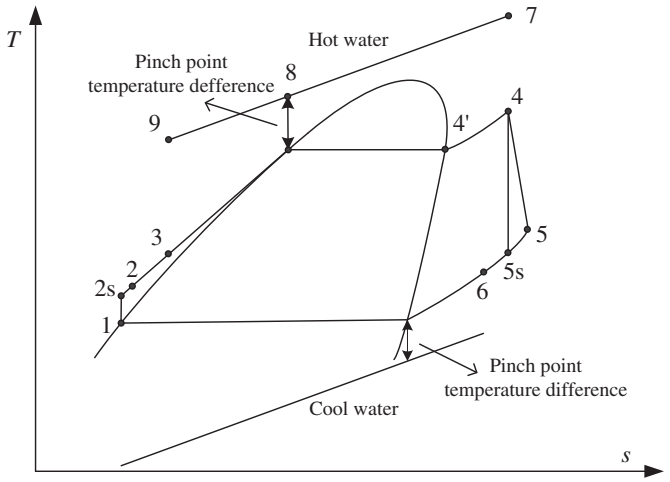

Fig. 2. *T*–*s* diagram of the solar-driven regenerative ORC system.

delivered to the turbine with high pressure vapor, where it expands and produces power by rotating the shaft connected to an electric generator. The turbine exhaust is condensed to liquid in the condenser by rejecting heat to environment.

The selection of the working fluids is very important for the cycle performance improvement. So, according to the work done by previous researchers, we evaluate a variety of substances comprehensively from the thermodynamic properties, cost, stability and so on, and finally select R245fa, R123, isobutane and R134a as the working fluids. The thermophysical properties and other characteristics of the selected working fluids are listed in Table 1.

3. Mathematical model and performance criteria

3.1. Solar energy collecting system

Flat-plate solar collectors are used to collect the solar radiation. As the solar radiation travels through the glass cover, it is absorbed

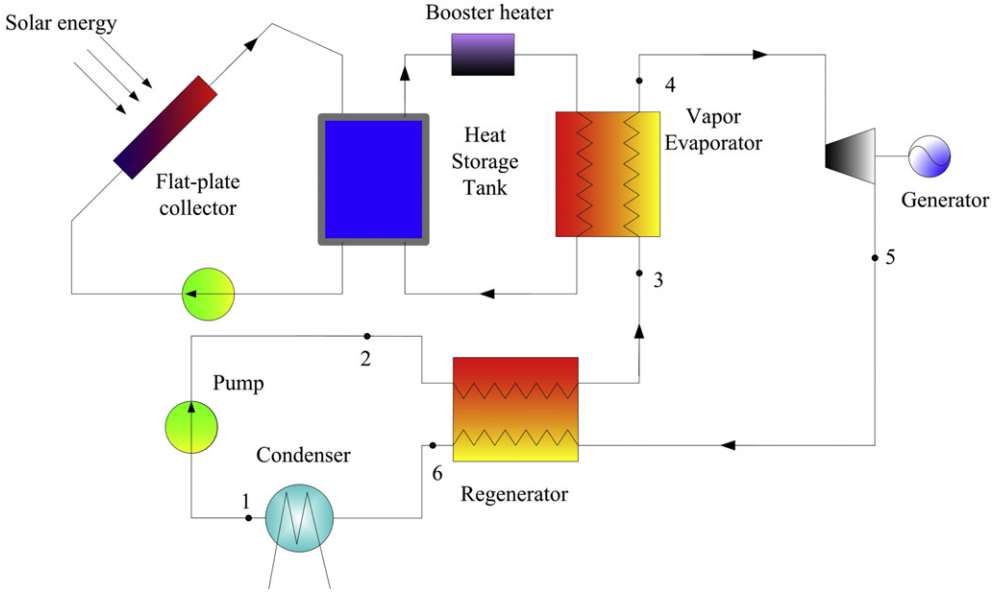

Fig. 1. Schematic diagram of the solar-driven regenerative ORC system.

Table 1
Properties of the fluids selected for the solar-driven regenerative ORC system.

Substance	Molecular mass /kg·kmol^{-1}	T_{crit}[a]/°C	P_{crit}[b]/MPa	T_{bp}[c]/°C	ODP[d]	GWP[e]/100year
R245fa	134.05	154.01	3.64	15.14	0	950
R123	152.93	183.68	3.668	27.82	0.020	77
Isobutane	58.12	134.70	3.63	−11.73	0	20
R134a	102.03	101.06	4.06	−26.07	0	1430

[a] T_{crit}: critical temperature.
[b] P_{crit}: critical pressure.
[c] T_{bp}: normal boiling point.
[d] ODP: ozone depletion potential.
[e] GWP: global warming potential.

by the absorber plate and carried away by the water in the tubes attached to the plate.

The hourly radiation falling on a tilted surface is given by Ref. [24]:

$$I_T = I_b R_b + I_d R_d + (I_b + I_d) R_r \tag{1}$$

where I_b and I_d are the hourly beam and diffuse radiation that the collector receives, and R_b, R_d, R_r are defined as tilt factors for different kinds of radiation, whose values are given by:

$$R_b = \frac{\cos(\theta)}{\cos(\theta_z)} = \frac{\sin\delta\sin(\phi-\beta) + \cos\delta\cos\omega\cos(\phi-\beta)}{\sin\phi\sin\delta + \cos\phi\cos\delta\cos\omega} \tag{2}$$

for beam radiation, where δ is the declination given by Cooper [25]

$$\delta = 23.45\sin\left[\frac{360}{365}(284+n)\right] \tag{3}$$

$$R_d = \frac{1+\cos\beta}{2} \tag{4}$$

for diffuse radiation, and

$$R_r = \rho\left(\frac{1-\cos\beta}{2}\right) \tag{5}$$

for reflected radiation falling on the surface of the plate.

The incident solar flux absorbed in the absorber plate is given by

$$S = I_b R_b (\tau\alpha)_b + [I_d R_d + (I_b + I_d) R_r](\tau\alpha)_d \tag{6}$$

where $(\tau\alpha)_b$ and $(\tau\alpha)_d$ represent the transmissivity–absorptivity product for beam and diffuse radiation falling on the collector, respectively.

The total loss coefficient U_L is made up of three parts, namely, the bottom, the top and the side loss coefficient:

$$U_L = U_b + U_t + U_s \tag{7}$$

Assuming that the flow of heat is one dimensional and steady, and the convective resistance at the bottom surface of the collector casing is neglected, the bottom loss coefficient is obtained as

$$U_b = \frac{k_i}{\delta_b} \tag{8}$$

where k_i is the thermal conductivity of the insulation and δ_b the thickness of the insulation.

If the dimensions of the absorber plate are $L_1 \times L_2$, the height of the collector casing is L_3 and the thickness of the insulation is δ_s, the side loss coefficient is given as

$$U_s = \frac{(L_1+L_2)L_3 k_i}{L_1 L_2 \delta_s} \tag{9}$$

The top loss coefficient is calculated by an empirical equation, which is proposed by Klein [26] as follows:

$$U_t = \left[\frac{M}{\left(\frac{C}{T_{pm}}\right)\left(\frac{T_{pm}-T_a}{M+f}\right)^{0.33}} + \frac{1}{h_w}\right]^{-1} + \left[\frac{\sigma\left(T_{pm}^2 + T_a^2\right)(T_{pm}+T_a)}{\frac{1}{\varepsilon_p + 0.05M(1-\varepsilon_p)} + \frac{(2M+f-1)}{\varepsilon_c}} - M\right] \tag{10}$$

In this study, the solar radiation travels through two glass plates ($M = 2$). T_{pm} and T_a stand for the average temperature and ambient temperature respectively. h_w is the convective heat transfer coefficient. In addition, parameter f and C can be determined by:

$$f = \left(1 - 0.04h_w + 0.0005h_w^2\right)(1 + 0.091M) \tag{11}$$

$$C = 365.9\left(1 - 0.00883\beta + 0.0001298\beta^2\right) \tag{12}$$

The collector efficiency factor F' is expressed as [27]:

$$F' = \frac{1}{W U_L\left\{\frac{1}{U_L[(W-D)\phi + D_o]} + \frac{1}{\pi D_i h_f}\right\}} \tag{13}$$

By introducing the collector heat-removal factor F_R, the useful heat gain rate for the collector is

$$F_R = \frac{m_{w1} C_p}{U_L A_p}\left[1 - \exp\left(-\frac{F' U_L A_p}{m_{w1} C_{pw}}\right)\right] \tag{14}$$

$$Q_u = F_R \cdot A_p \cdot \left[S - U_L \cdot \left(T_{fi} - T_a\right)\right] \tag{15}$$

where, A_p is the thermal-absorption area of the collector. The water flows into the collector through the tubes at the temperature T_{fi}.

3.2. Thermal storage system

In this system, we use a sensible thermal storage system to store the collected solar energy. To simplify the model, it is assumed that the water in the insulated water storage tank is completely mixed with the water flowing back into the tank from the collector and the vapor evaporator as shown in Fig. 3. Moreover, we assume that the ambient temperature T_a is constant and the loss of the water tank is considered. The following equation can be obtained from the energy balance in the tank [24]

$$\left[(\rho V C_p)_w + (\rho V C_p)_t\right]\frac{dT}{dt} = Q_u - Q_{load} - (UA)_t \cdot (T_L - T_a) \tag{16}$$

where $(\rho C_p V)_w$ stands for the heat capacity of the water in the tank, $(\rho C_p V)_t$, the heat capacity of the tank material (steel in this case), T_a, the ambient temperature around the tank, and $(UA)_t$, the product of the overall heat transfer coefficient and surface area of the tank. Based on the assumption that Q_u, Q_{load} and T_a are constants within a reasonably small interval of time (1 h or less), Eq. (16) can be integrated to the following form

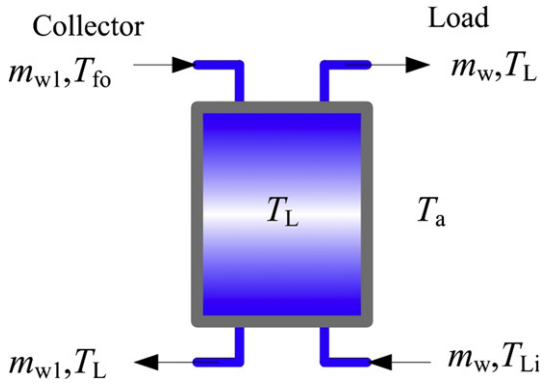

Fig. 3. Schematic diagram of the heat storage tank.

$$\frac{Q_u - Q_{load} - (UA)_t \cdot (T_L - T_a)}{Q_u - Q_{load} - (UA)_t \cdot (T_{Li} - T_a)} = \exp\left[- \frac{(UA)_t \cdot t}{(\rho V C_p)_e} \right] \tag{17}$$

where the sum of the two heat capacities is replaced by a single $(\rho C_p V)_e$ and the initial condition is presumed to be $t = 0$ and $T_L = T_{Li}$.

Furthermore, Q_u, Q_{load} and Q_{loss}, which represent the useful gain from the solar collectors, the energy discharged to power subsystem and the loss in the storage tank, respectively, can be calculated as

$$Q_u = m_w C_{pw} (T_{fo} - T_L) \tag{18}$$

$$Q_{load} = m_w C_{pw} (T_L - T_i) \tag{19}$$

$$Q_{loss} = (UA)_t \cdot (T_L - T_a) \tag{20}$$

3.3. Organic Rankine cycle system

The organic Rankine cycle system is modeled based on the laws of mass and energy conservations. To simplify the theoretical analysis, some assumptions are made as follows:

(1) The system reaches a steady state.
(2) The pressure drops in vapor evaporator, regenerator, condenser, and the connection tubes are neglected.
(3) The working fluid at the condenser outlet is saturated liquid, and there exists a temperature difference of condenser, namely, the temperature difference of condensed temperature and cooling water temperature.
(4) The pump and the turbine have a given isentropic efficiency, respectively.

For the turbine, the isentropic efficiency can be expressed as

$$\eta_T = \frac{h_4 - h_5}{h_4 - h_{5s}} \tag{21}$$

The power output can be given by

$$W_T = m_R (h_4 - h_5) \tag{22}$$

For the pump, the isentropic efficiency can be expressed as:

$$\eta_P = \frac{h_{2s} - h_1}{h_2 - h_1} \tag{23}$$

The pump power consumption is given by

$$W_P = m_R (h_2 - h_1) \tag{24}$$

In the vapor evaporator, the heat addition into the power cycle is extracted from the thermal storage tank, which implies:

$$Q_{load} = Q_{in} = m_R (h_4 - h_3) \tag{25}$$

In the condenser, the rejected heat is expressed as

$$Q_{out} = m_R (h_6 - h_1) \tag{26}$$

In the regenerator, the energy balance is expressed as:

$$m_R (h_3 - h_2) = m_R (h_5 - h_6) \tag{27}$$

3.4. System performance criteria

Previous researchers in this field have defined the system efficiency as the ratio of the power output to the useful heat gain rate from the collector to evaluate the overall system performance. This is fairly advisable to evaluate the instantaneous performance of the solar-driven power cycle at a given time of the day.

The instantaneous efficiency is defined as:

$$\eta_{instant} = \frac{W_{net}}{Q_u} \tag{28}$$

However, when determining the system performance over a period of time or a whole day, such assessment index suffers from intrinsic limitations. On one hand, the useful heat gain Q_u varies greatly with the radiation intensity, reaching its peak in midday and dropping sharply towards zero when the sun sets. On the other hand, for the system equipped with a thermal storage tank, the power generation could be sustained long after sunset. Then the instantaneous efficiency would be unable to evaluate the system performance in the evening or at night. Therefore, we introduce an alternative to demonstrate the whole-day performance of the system. A daily average efficiency is defined to replace instantaneous efficiency by integrating W_{net} and Q_u over a period of time, which is expressed as follows:

$$\eta_d = \frac{\int_{t_1}^{t_2} W_{net}(t)\mathrm{d}t}{\int_{t_1}^{t_2} Q_u(t)\mathrm{d}t} \tag{29}$$

4. Results and discussion

In this section, we present the numerical simulation of the solar-driven regenerative organic Rankine cycle using the mathematical models established above. Xi'an city in China (N34.27°, E108.9°) is selected as the case city, and June 1 with a wind speed of 2 m s^{-1} as the case day. The thermophysical properties of working fluid are calculated by REFPROP [28] developed by the National Institute of Standards and Technology. The initial calculation conditions are listed in Table 2 to simulate the solar-driven regenerative ORC.

4.1. The daily simulation of the solar-driven regenerative organic Rankine cycle

Fig. 4 shows the variations of incident solar flux, useful heat gain, water temperature in storage tank and ambient temperature with the time over a day under the condition that the load of the storage tank is constant. Being similar to the incident solar flux, the

Table 2
Design conditions of the solar-driven regenerative ORC system.

Name	Value	Unit
Ambient temperature	20	°C
Ambient pressure	0.1	MPa
Inclination angle of solar collector	34.27	°
External diameter of collector tube	0.018	m
Inner diameter of collector tube	0.014	m
Size of a single solar-collecting plate	1.76 (1.6 × 1.1)	m^2
Number of solar-collecting plates	300	/
External diameter of water tank	2.1	m
Inner diameter of water tank	1.7	m
Water tank height	2.0	m
Water tank wall thickness	0.006	m
Insulation layer thickness	0.2	m
Number of water tank	3	/
Pinch point temperature difference	8	°C
Condensation temperature	20	°C
Temperature difference of condenser	5	°C
Temperature difference of regenerator	5	°C
Pump efficiency	70	%
Turbine isentropic efficiency	70	%

useful heat gain varies greatly with the radiation intensity, reaching its peak in midday and dropping sharply towards zero when the sun sets. The ORC system could be operated normally after sunset owing to the thermal storage tank. It can be observed that the useful heat gain increases after 7:00 am and when it is greater than the load demand, the solar collector provides more energy and the surplus heat is stored in the thermal storage tank, resulting in an increase in tank water temperature. The useful heat gain reaches its peak at midday, but the peak value of water temperature in storage tank lags behind the useful heat gain due to the thermal storage. After about 15:00 pm the useful heat gain is less than load demand, the tank water temperature begins to decrease. When there is little solar radiation after 17:00, the thermal storage tank releases the stored heat to provide energy to the bottoming ORC.

Assuming that turbine inlet temperature, turbine inlet pressure and condensation temperature are unchanged, the variations of the net power output based on the four different working fluids with the time over a day are shown in Fig. 5. The net power output increases steadily from 8:00 to 15:00 and then decreases, which has the same trend as the water temperature in storage tank. This finding is understandable because the increasing water temperature in storage

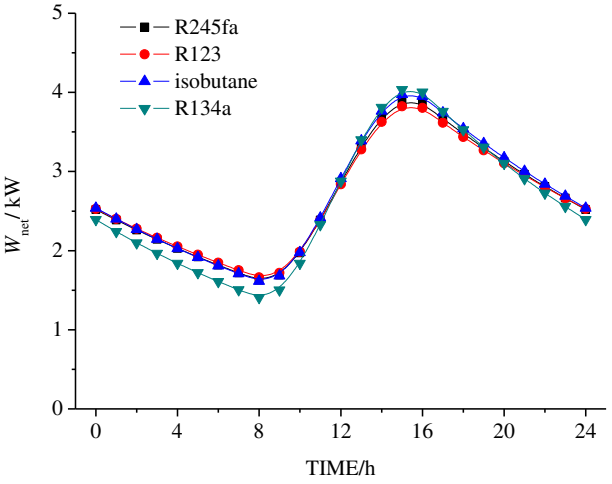

Fig. 5. Variation of net power output with time over a day using different fluids.

tank results in an increase in mass flow rate of working fluids generated in the vapor evaporator with unchanged other thermodynamic parameters, i.e. the mass flow rate of working fluids across the turbine increases. Considering the pump power consumption, the net power output is different during the early and late hours for all working fluids.

4.2. Sensitivity analyses of key thermodynamic parameters

Three key thermodynamic parameters, turbine inlet temperature, turbine inlet pressure and condensation temperature are selected to examine the system performance. We analyze the effects of key performance parameters on the system performance at an instant moment (14 o'clock). In the sensitivity analyses, one thermodynamic parameter is varied, whereas other parameters of the solar-driven regenerative ORC system are kept constant as those in Table 2.

4.2.1. Effects of turbine inlet temperature on the ORC system

Assuming that the different working fluids at turbine inlet were in superheated state with constant turbine inlet pressure respectively (R245fa: 0.34 MPa; R123: 0.21 MPa; isobutane: 0.68 MPa; R134a: 1.31 MPa) and the condensation temperature was 20 °C.

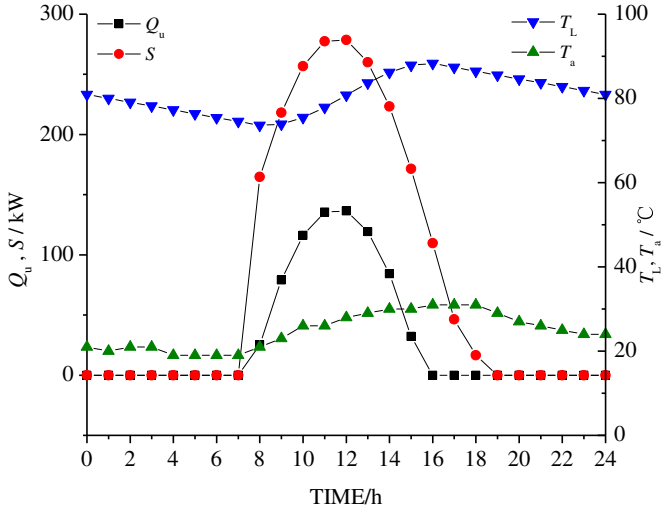

Fig. 4. Variations of S, Q_u, T_L and T_a with time over a day.

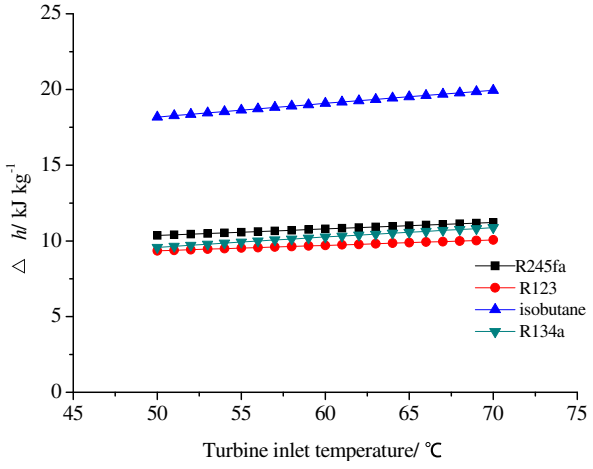

Fig. 6. Variation of enthalpy drop across turbine with turbine inlet temperature.

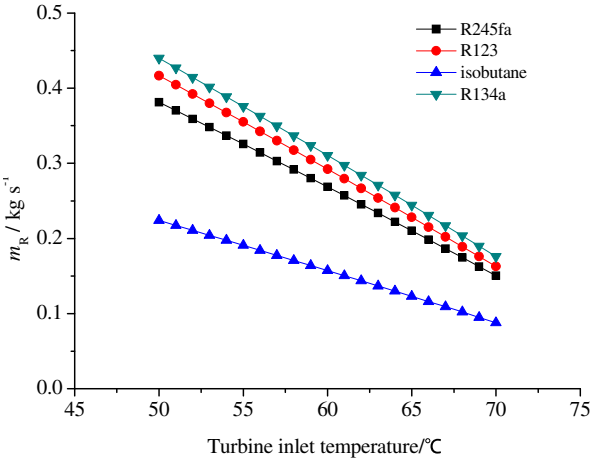

Fig. 7. Variation of mass flow rate in ORC with turbine inlet temperature.

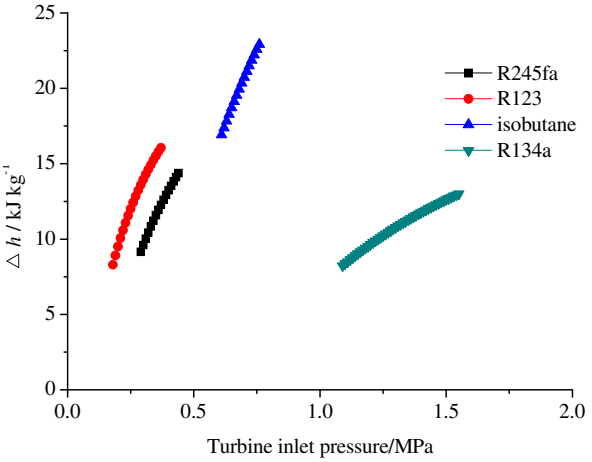

Fig. 9. Variation of enthalpy drop across turbine with turbine inlet pressure.

Figs. 6–8 respectively illustrate the variations of enthalpy drop across turbine, mass flow rate in ORC and net power output with turbine inlet temperature. An increase in turbine inlet temperature leads to an increase in enthalpy drop across turbine and a decrease in mass flow rate. Because with the unchanged evaporation temperature and pinch point temperature difference, a higher turbine inlet temperature results in a larger enthalpy difference and enables the mass flow rate in the evaporator to decrease according to energy balance. Since the effect of the decreasing mass flow rate is much greater than that of the increasing enthalpy drop across the turbine, the net power output considering the pump consumption power decreases.

According to the previous results above, the evaporation pressure of the four different working fluids can be ordered from high to low as R134a, isobutane, R245fa and R123. Since we prefer lower evaporation pressure and lower mass flow rate considering safe operation and economic efficiency, R245fa and R123 seem to be more suitable for the ORC system.

4.2.2. Effects of turbine inlet pressure on the ORC system

Assuming that the turbine inlet temperature is 70 °C and condensation temperature 20 °C. Figs. 9 and 10 respectively show that the enthalpy drop across turbine increases and the mass flow rate with different working fluids decreases with an increase in turbine inlet pressure. Because the vapor evaporator temperature can increase with an increase in turbine inlet pressure, the water temperature (hot side) leaving vapor evaporator is elevated with the limitation of pinch point temperature difference and the heat transfer rate in vapor evaporator falls, resulting in a decrease in mass flow rate in ORC. Fig. 11 shows the variation of net power output with turbine inlet pressure. As the turbine inlet pressure increases, the net power output increases firstly, reaches to its peak and declines when the enthalpy gains across turbine do not make up for the decrease in mass flow rate of working fluid across the turbine for different working fluids.

Since the differences of net power output among four different fluids are not very great, R123 or R245fa could be good candidate working fluids owing to their lower operating pressure.

4.2.3. Effects of condensation temperature on the ORC system

The condensation temperature also is another important parameter to evaluate the system performance. We set the condensation temperature changing from 20 °C to 30 °C under the condition that the fluid at turbine inlet is saturated vapor state. It is obvious that the enthalpy drop across turbine decreases and the mass flow rate is unchanged as the condensation temperature increases as shown in Figs. 12 and 13. Meanwhile, the net power output also presents a decreasing tendency with the rising condensation temperature owing to the decreasing enthalpy drop across turbine as shown in Fig. 14.

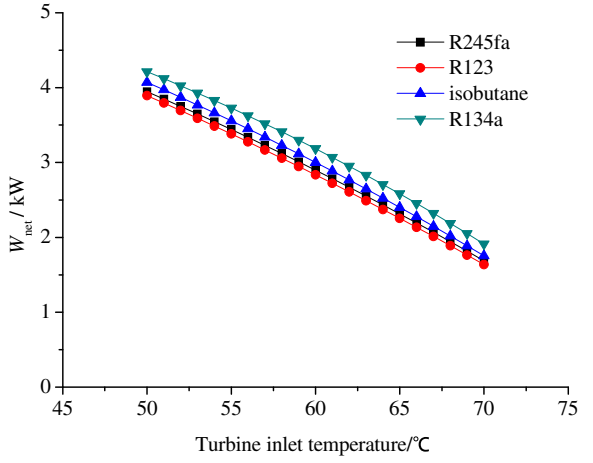

Fig. 8. Variation of net power output with turbine inlet temperature.

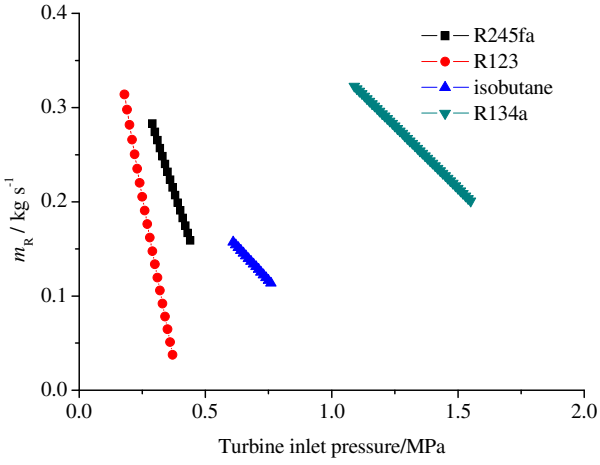

Fig. 10. Variation of mass flow rate in ORC with turbine inlet pressure.

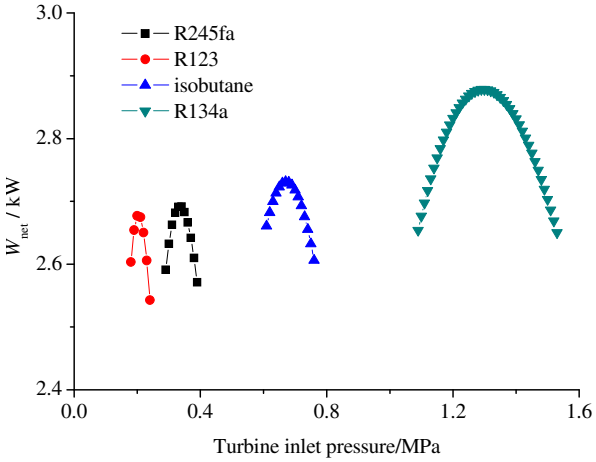

Fig. 11. Variation of net power output with turbine inlet pressure.

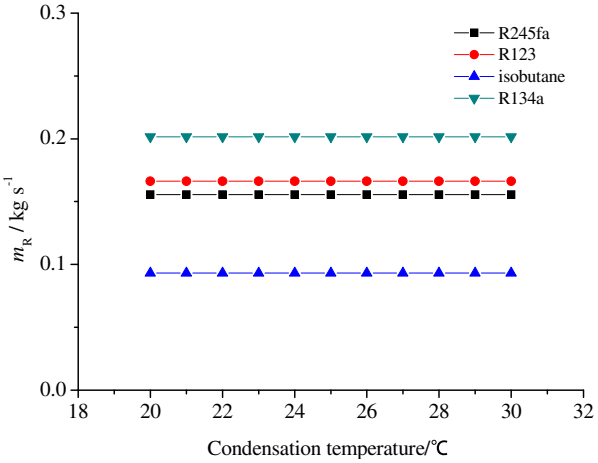

Fig. 13. Variation of mass flow rate in ORC with condensation temperature.

4.3. Effects of T_T, P_T and T_{cond} on daily average efficiency

The modified system efficiency, daily average efficiency η_d, is the key criterion to evaluate the system performance. Fig. 15 shows that the daily average efficiency increases gradually with an increase in turbine inlet temperature, implying that over a whole day the increasing enthalpy drop across turbine plays a dominating part to enhance daily average efficiency compared with the decreasing mass flow rate of working fluid. It can be indicated in Fig. 16 that as the turbine inlet pressure increases, the daily average efficiency also increases, implying that over a whole day the increasing enthalpy drop across turbine plays a dominating part to enhance daily average efficiency. Fig. 17 shows the daily average efficiency decreases gradually with an increase in condensation temperature owing to the decreasing enthalpy drop across turbine with an increase in turbine back pressure.

5. Optimization

According to the preceding parametric analysis, we must conduct the parametric optimization to get the optimum system performance. The modified system efficiency, daily average efficiency, is selected as the objective function. Two key thermodynamic parameters, namely, turbine inlet temperature and turbine inlet pressure, are selected as the decision variables. The genetic algorithm is employed to optimize the system performance to find the optimum group of the two parameters and to get the optimal system performance.

5.1. Optimization method – genetic algorithm

Firstly introduced by John Holland [29], the genetic algorithm is based on the theory of the natural selection in the biological genetic progress which was developed by Charles Darwin. The GA considers every parameter as a gene as well as a solution as a chromosome by encoding them as binary numbers. Different combinations of genes make up a population of variable chromosome-like structure. Before the GA, a group of chromosomes are given, called the original population. The better approximations in the original population generate a new generation and the better approximations to potential results are selected as the new population. Then the new population continues to generate next generation and stops when the population converges to the optimal result. In the GA, the fitness value is assessed by the fitness function. Larger fitness value corresponds to better adaptability of the chromosome- like structure. In this study, the daily system efficiency is chosen as the fitness function.

The operators of the GA consist of selection, crossover and mutation. First, the selection operator selects parents to generate

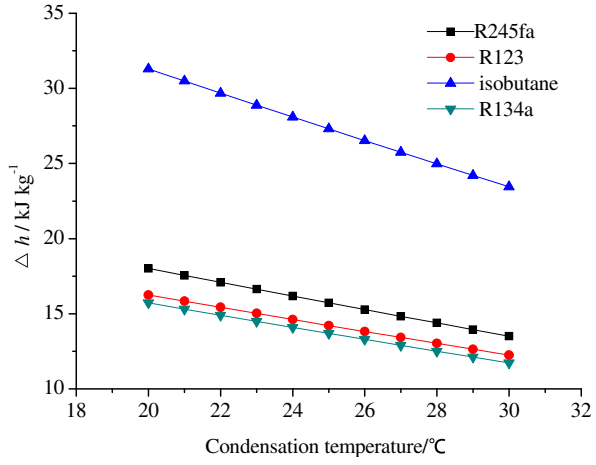

Fig. 12. Variation of enthalpy drop across turbine with condensation temperature.

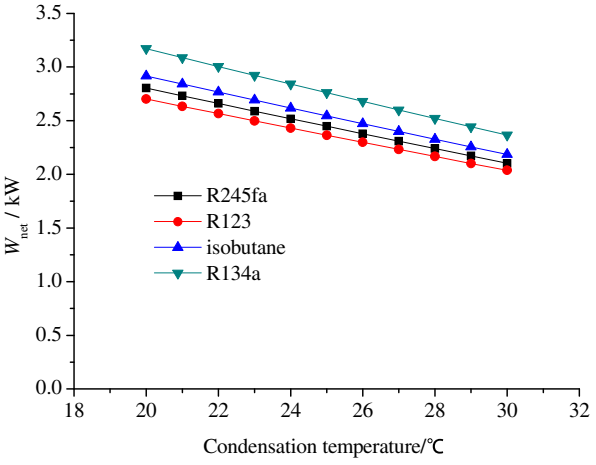

Fig. 14. Variation of net power output with condensation temperature.

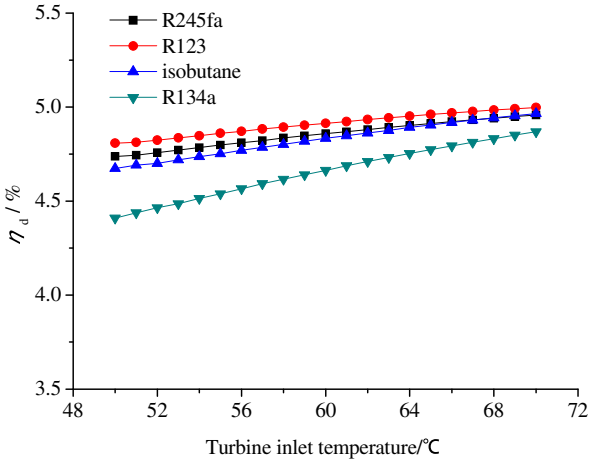

Fig. 15. Variation of daily average efficiency of system with turbine inlet temperature.

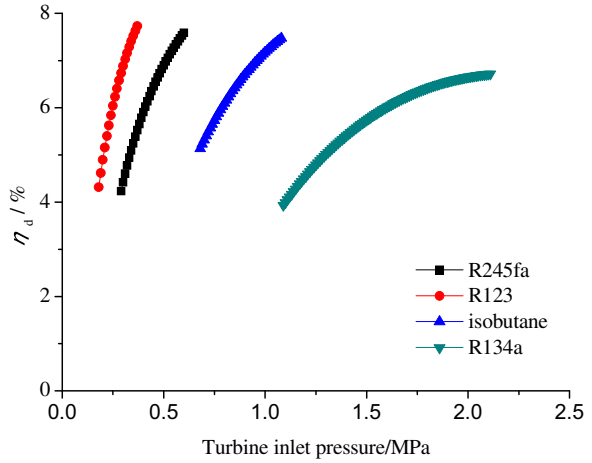

Fig. 16. Variation of daily average efficiency of system with turbine inlet pressure.

the children of solutions. When chosen to generate the next generation, the parents are conducted by crossover operator at a certain probability. In the process of the optimization, mutation is a non-ignorable operator because only selection and crossover operators producing new solutions can tend to converge rapidly

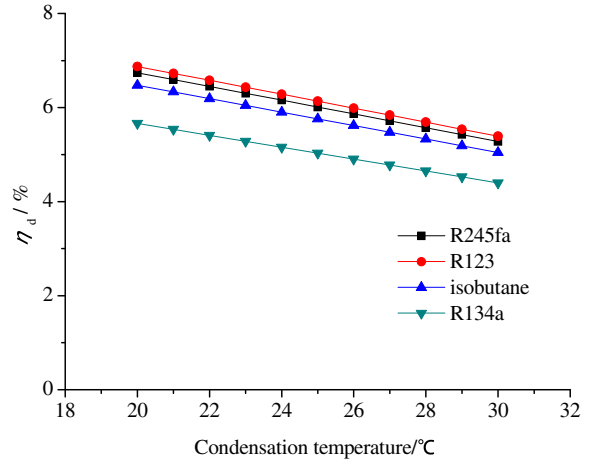

Fig. 17. Variation of daily average efficiency of system with condensation temperature.

Table 3
Data of the parameter optimization.

Fluids	R245fa	R123	Isobutane	R134a
Population size	10			
Crossover probability	0.8			
Mutation probability	0.02			
Stop generation	200			
The range of turbine inlet temperature/°C	50–70			
The range of turbine inlet pressure/MPa	0.20–0.80	0.15–0.50	0.40–1.20	1.00–2.30
Condensation temperature/°C	20			

Table 4
Optimization results of the solar-driven regenerative ORC system.

Fluid	T_T/°C	P_T/MPa	η_d/%
R245fa	69.99	0.603	7.70
R123	69.84	0.369	7.79
Isobutane	70.00	1.075	7.56
R134a	69.96	2.093	6.80

and lose some potential solutions. Considering actual operation, the mutation operator is to change the original binary code into its opposite code with a small probability named mutation probability.

5.2. Optimization results

In this solar-driven regenerative organic Rankine cycle, the ranges of the key thermodynamic parameters and the operation parameters of GA are listed in Table 3. The maximum value of turbine inlet temperature is set to be 70 °C to enable the system to operate stably and the condensation temperature is 20 °C. Table 4 lists the results of parameter optimization with different working fluids. It is observed that to achieve the optimal daily average efficiency, turbine inlet temperature is close to the maximum value and turbine inlet pressure is close to the saturation pressure corresponding to the best turbine inlet temperature. It is implied that under the actual constraints, a higher turbine inlet temperature with saturated vapor state could obtain a better system performance. Compared with other working fluids, R123 has the highest system performance with the lowest optimal turbine inlet pressure which is beneficial to the safe operation of the solar-driven regenerative ORC system.

6. Conclusions

In this study, we carried out the simulation of a solar-driven regenerative organic Rankine cycle based on flat-plate solar collectors using different organic working fluids. By establishing the mathematical model to simulate the system under steady-state conditions, we analyzed the influences of the key thermodynamic parameters on the system performance. Finally, we employ genetic algorithm to conduct the parameter optimization with the daily average efficiency as its objective function. The main conclusions drawn from the study are summarized as follows:

(1) By introducing a thermal storage tank into the system, the solar-driven regenerative organic Rankine cycle can achieve a continuous and stable operation over a long time. The daily average efficiency based on W_{net}–Q_u ratio by integrating both power and useful heat gain over a period of time is able to provide a more reasonable evaluation for the system performance.

(2) Increasing the enthalpy drop across turbine could increase daily average efficiency. Under the actual constraints, enhancing the thermodynamic parameters at turbine inlet or lowering the turbine back pressure could improve the system performance. The parameter optimization also implies that a higher turbine inlet temperature with saturated vapor state could obtain a better system performance.
(3) Compared with other working fluids, R245fa and R123 could prove to be the most suitable working fluids for the system due to their high system performance and low operation pressure.

Acknowledgements

The authors gratefully acknowledge the financial support by the National Natural Science Foundation of China (Grant No. 51106117) and the Natural Science Foundation of Shaanxi Province (Grant No. 2011JQ7002).

References

[1] H. Chen, D.Y. Goswami, E. Stefanakos, A review of thermodynamic cycles and working fluids for the conversion of low-grade heat, Renew. Sust. Energ. Rev. 14 (2010) 3059–3067.
[2] B.F. Tchanche, Gr. Lambrinos, A. Frangoudakis, G. Papadakis, Low-grade heat conversion into power using organic Rankine cycles – a review of various applications, Renew. Sust. Energ. Rev. 15 (2011) 3963–3979.
[3] J. Li, G. Pei, J. Ji, Optimization of low temperature solar thermal electric generation with Organic Rankine Cycle in different areas, Appl. Energ. 87 (2010) 3355–3365.
[4] G. Pei, J. Li, J. Ji, Analysis of low temperature solar thermal electric generation using regenerative Organic Rankine Cycle, Appl. Therm. Eng. 30 (2010) 998–1004.
[5] S. Quoilin, M. Orosz, H. Hemond, V. Lemort, Performance and design optimization of a low-cost solar organic Rankine cycle for remote power generation, Sol. Energy 85 (2011) 955–966.
[6] X.D. Wang, L. Zhao, J.L. Wang, W.Z. Zhang, X.Z. Zhao, W. Wu, Performance evaluation of a low-temperature solar Rankine cycle system utilizing R245fa, Sol. Energy 84 (2010) 353–364.
[7] X.D. Wang, L. Zhao, J.L. Wang, Experimental investigation on the low-temperature solar Rankine cycle system using R245fa, Energ. Convers. Manag. 52 (2011) 946–952.
[8] C.B. Joan, L.V. Jesus, L. Eduardo, R. Silvia, C. Alberto, Modelling and optimisation of solar organic Rankine cycle engines for reverse osmosis desalination, Appl. Therm. Eng. 28 (2008) 2212–2226.
[9] M.A. Sharaf, A.S. Nafey, García-Rodríguez Lourdes, Exergy and thermo-economic analyses of a combined solar organic cycle with multi effect distillation (MED) desalination process, Desalination 272 (2011) 135–147.
[10] A.S. Nafey, M.A. Sharaf, García-Rodríguez Lourdes, Thermo-economic analysis of a combined solar organic Rankine cycle-reverse osmosis desalination process with different energy recovery configurations, Desalination 261 (2010) 138–147.
[11] B.F. Tchanche, Gr. Lambrinos, A. Frangoudakis, G. Papadakis, Exergy analysis of micro-organic Rankine power cycles for a small scale solar driven reverse osmosis desalination system, Appl. Energ. 87 (2010) 1295–1306.
[12] D. Manolakos, G. Papadakis, Essam Sh. Mohamed, S. Kyritsis, K. Bouzianas, Design of an autonomous low-temperature solar Rankine cycle system for reverse osmosis desalination, Desalination 183 (2005) 73–80.
[13] D. Manolakos, G. Kosmadakis, S. Kyritsis, G. Papadakis, On site experimental evaluation of a low-temperature solar organic Rankine cycle system for RO desalination, Sol. Energy 83 (2009) 646–656.
[14] G. Kosmadakis, D. Manolakos, G. Papadakis, Parametric theoretical study of a two-stage solar organic Rankine cycle for RO desalination, Renew. Energ. 35 (2010) 989–996.
[15] G. Kosmadakis, D. Manolakos, S. Kyritsis, G. Papadakis, Design of a two stage Organic Rankine Cycle system for reverse osmosis desalination supplied from a steady thermal source, Desalination 250 (2010) 323–328.
[16] M.D. Agustín, G.R. Lourdes, Double cascade organic Rankine cycle for solar-driven reverse osmosis desalination, Desalination 216 (2007) 306–313.
[17] M.D. Agustín, G.R. Lourdes, J.R. Vicente, Preliminary design of a solar thermal-powered seawater reverse osmosis system, Desalination 216 (2007) 292–305.
[18] M.D. Agustín, G.R. Lourdes, Preliminary design of seawater and brackish water reverse osmosis desalination systems driven by low-temperature solar organic Rankine cycles (ORC), Energ. Convers. Manag. 51 (2010) 2913–2920.
[19] B.F. Tchanche, G. Papadakis, G. Lambrinos, A. Frangoudakis, Fluid selection for a low-temperature solar organic Rankine cycle, Appl. Therm. Eng. 29 (2009) 2468–2476.
[20] R. Rayegan, Y.X. Tao, A procedure to select working fluids for Solar Organic Rankine Cycles (ORCs), Renew. Energ. 36 (2011) 659–670.
[21] X.D. Wang, L. Zhao, Analysis of zeotropic mixtures used in low-temperature solar Rankine cycles for power generation, Sol. Energy 83 (2009) 605–613.
[22] J.L. Wang, L. Zhao, X.D. Wang, A comparative study of pure and zeotropic mixtures in low-temperature solar Rankine cycle, Appl. Energ. 87 (2010) 3366–3373.
[23] J.J. Bao, L. Zhao, W.Z. Zhang, A novel auto-cascade low-temperature solar Rankine cycle system for power generation, Sol. Energy 85 (2011) 2710–2719.
[24] S. Sukhatme, Solar Energy-principles of Thermal Collection and Storage, Tata McGraw-Hill Publishing Company Limited, India, 1984.
[25] P. Cooper, The absorption of solar radiation in solar stills, Sol. Energy 12 (1969) 333–346.
[26] S.A. Klein, Calculation of flat-plate collector loss coefficient, Sol. Energy 17 (1975) 79–80.
[27] J.A. Duffie, W.A. Beckman, Solar Engineering of Thermal Processes, second ed., Wiley-Interscience, New York, 1991.
[28] NIST Standard Reference Database 23, NIST Thermodynamic and Transport Properties of Refrigerants and Refrigerant Mixtures REFROP, Version 9.0 (2010).
[29] J. Holland, Adaptation in Nature and Artificial Systems: An Introductory Analysis with Applications to Biology, Control and Artificial Intelligence, MIT Press, Massachusetts, 1992.